Selective Neurodegeneration of the Hippocampus Caused by Chronic Cerebral Hypoperfusion: F-18 FDG PET Study in Rats

석 사 학 위 논 문

Selective Neurodegeneration of the Hippocampus Caused by Chronic Cerebral Hypoperfusion : F-18 FDG PET Study in Rats

계 명 대 학 교 대 학 원

의 학 과

이 정 인

지도교수 김 해 원

2 0 2 1 년 2 월

이 정 인

2021년 2월

Selective Neurodegeneration of the Hippocampus Caused by Chronic Cerebral Hypoperfusion : F-18 FDG PET Study in Rats

지도교수 김 해 원

이 논문을 석사학위 논문으로 제출함

2021년 2월

계 명 대 학 교 대 학 원

의 학 과

이 정 인

이정인의 석사학위 논문을 인준함

주 심 홍 정 호

부 심 김 해 원

부 심 김 신

계 명 대 학 교 대 학 원

２０２１년 ２월

Acknowledgement

본 논문을 준비하고 제출하는데 있어서 정말 많은 시간이 들었고, 많은 분들의 도움이 있었기에 가능했습니다. 긴 시간 동안 항상 옆에서 연구 방향 제시와 부족한 부분들을 채워주시고 바쁘신 가운데에도 세세한 부분까지 지도해 주신 지도 교수님 김해원 교수님께 머리 숙여 깊이 감사를 드립니다. 그리고 바쁘신 일정에도 논문의 교정, 심사까지 정성껏 지도해주시고 심사위원을 맡아주신 홍정호 교수님, 김신 교수님께 이 글을 통해 다시 한 번 진심으로 감사의 마음을 드립니다. 또한 학위과정 중에 언제나 도움을 주고 격려해 준 의과학 연구소 선생님들께도 감사의 말씀 전합니다. 학위과정은 아무것도 모르는 저에게는 힘든 시간이었지만, 뒤돌아보면 제가 많이 성장 할 수 있는 시간이었습니다. 아직 많이 부족하지만 앞으로도 계속 정진하여 더 나은 연구자가 될 수 있도록 노력하겠습니다.

마지막으로 늘 믿어주시고 깊고 넓은 사랑으로 보듬어주신 부모님께 이 논문을 바칩니다.

2021년 2월

이 정 인

Table of Contents

List of Tables

List of Figures

1. Introduction

Alzheimer's disease (AD) accounts for 60% to 70% of cases of dementia, which according to current estimates, will affect up to 81.1 million patients worldwide by 2040 (1). Deposition of amyloid beta (Aβ) and neurofibrillary tangles are the main pathological hallmarks of AD, which are respectively caused by aggregation of Aβ peptides and hyperphosphorylated tau (p-tau) in the brain (2, 3). Although the cause of AD pathology has not been clearly identified, previous studies have reported the relationship between cerebral hypoperfusion and AD pathology (4); therefore, cerebral hypoperfusion may be a predisposing factor in the pathological progression of AD. This is supported by the fact that vascular risk factors that cause cerebral hypoperfusion, such as hypertension, diabetes, hypercholesterolemia, and smoking, are also risk factors of AD (5). Further, the small vessels of the neocortex in AD patients are frequently narrowed, degenerated, and contain Aβ (6, 7), suggesting that cerebrovascular factors play a pivotal role in AD development. In addition, cerebral hypoperfusion is known to potentiate other processes associated with AD such as mitochondrial failure, oxidative stress, and neuroinflammation (8, 9).

Cerebral hypoperfusion can occur in two patterns, acute or chronic, depending on the rate at which cerebral vessels narrow; both cause cognitive deficits in various degrees (10). While acute cerebral hypoperfusion leads to an infarction within approximately 3 h via necrosis of neuronal cells (11), chronic cerebral hypoperfusion (CCH) causes neurodegeneration over a period of months to years through neuronal apoptosis without infarction (12). The important role of CCH in AD has already emerged at the vanguard of neurology research (13).

Recent *in vivo* studies have revealed that CCH accelerates AD pathology, including Aβ aggregation and cognitive dysfunction (14, 15). In turn, Aβ aggregation has been shown to exacerbate inefficient microcirculation and cause blood brain barrier disruption, indicating a vicious cycle between CCH and AD pathology (16). However, it is not clear which cerebral regions are affected by CCH to cause AD pathology.

F-18 fluorodeoxyglucose (FDG) positron emission tomography (PET) is a minimally invasive diagnostic brain imaging modality that is used to evaluate regional cerebral glucose metabolism. F-18 FDG uptake on PET reflects regional glucose consumption and synaptic function in the brain (17, 18), and is influenced by various factors, including reduced synaptic activity, neuronal disruption by Aβ plaques, and disconnection between histopathologically affected regions and functionally associated areas (19, 20). It has been reported that decreased glucose metabolism in specific cerebral regions is an important indicator for the detection of early AD (21). Thus, serial evaluation of regional cerebral glucose metabolism with F-18 FDG PET will help to identify the specific cerebral regions initially affected by CCH. The purpose of this study was to identify the cerebral regions that are affected by CCH using F-18 FDG PET, and to evaluate the development of AD pathology in a rat model of CCH.

2. Materials and Methods

2.1. Animals:

Eight-week-old male Wistar rats (250-300 g body weight) purchased from Central Lab Animal Korea, Inc. were used for this study. They were kept in standard cages at a temperature of 22-24 ℃ with 12 h light/12 h dark cycles (8:00 lights on) and controlled humidity (55-60%). Food and water were freely accessible. The surgery, cerebral blood flow (CBF), 2,3,5-triphenyltetrazolium chloride (TTC) assay, F-18 FDG PET, western blot analysis, and Y-maze tests were performed according to the schedule illustrated in Figure 1. All experiments in this study were performed in accordance with the guidelines for animal research from the National Institutes of Health. The Keimyung University Institutional Ethics Committee (Daegu, Korea) approved all the animal experiments (KM-2019-13R1).

2.2. Bilateral common carotid artery ligation surgery:

The rat model of CCH was established as previously described (22). Briefly, the bilateral common carotid artery (CCA) was doubly ligated in 22 Wistar rats (CAL group), whereas 22 sham-operated rats were exposed to the same procedures without CCA ligation (control group). Rats were anaesthetized using 4.0% isoflurane in N_2O/O_2 (70:30) and maintained with 2.0% isoflurane in N_2O/O_2 (70:30). The core temperature was maintained between 37 ℃ and 38 ℃ throughout the entire procedure. A small incision was carefully performed to facilitate the

separation of the bilateral CCA from the surrounding tissues. Polylysine-coated nylon (Nylon Monofilament Suture, Fine Science Tools Inc., Foster City, USA) was tightened around the CCA stump. In the control group, only anesthesia and vascular dissection were performed. For postsurgical care, rats were placed into separate cages.

2.3. Laser-Doppler flowmetry:

The CBF was measured in 15 rats in each group (CAL and control) using laser-Doppler flowmetry (OMEGA FLOW FLO-C1 BV, OMEGAWABE, Tokyo, Japan), as previously reported (22, 23). Under deep anesthesia with 4.0% isoflurane in N_2O/O_2 (70:30), the right skull was reflected. A laser-Doppler flowmetry probe was fixed perpendicularly to the skull at 1 mm posterior and 2.5 mm lateral to the bregma using dental resin. The CBF recordings were obtained just before (baseline), and at 30 min, 3 days, 14 days, 1 month, and 3 months after surgery. The CBF ratio (%) was calculated as a percentage of the baseline CBF before the surgery.

2.4. TTC assay:

To evaluate the cerebral infarction, a TTC assay was performed 1 day after bilateral CCA ligation. Seven rats from each group (control gorup and CAL group) were sacrificed. Their brains were removed and sliced into five coronal sections with a thickness of 2 mm. These sections were immersed in prewarmed 2% TTC (Sigma-Aldrich, Steinheim, Germany) in saline for 15 min and then fixed in 4% paraformaldehyde overnight. White regions of the brain indicated

cerebral infarct areas, whereas normal tissue regions were stained red by TTC.

2.5. F-18 FDG PET:

To evaluate cerebral glucose metabolism, 15 rats from each group (control group and CAL group) underwent an F-18 FDG PET at 1 month and 3 months after bilateral CCA ligation using the Triumph II PET/CT system (Lab-PET8; Gamma Medica-Ideas, Waukesha, WI, USA). Rats were kept fasting for 12 h before the PET scan. They were anaesthetized using 2.0% isoflurane in N_2O/O_2 (70:30), and injected with approximately 37 MBq of F-18 FDG via the tail vein. The rats underwent PET scanning approximately 30 min after F-18 FDG injection to acquire whole-brain images; the PET scan lasted for 20 min. The acquired data were assumed to represent cerebral glucose metabolism. For spatiotemporal quantification of the cerebral glucose metabolism, a volume-of interest (VOI) analysis was performed for each scan using the PMOD software package (PMOD Technologies, Ltd., Zurich, Switzerland) in conjunction with the W. Schiffer rat brain template and atlas, as previously described (22, 24). PMOD was used to transform each of the rat brain PET datasets to the appropriate space, and the W. Schiffer VOI brain atlas was automatically applied to measure the F-18 FDG uptake to acquire standardized F-18 FDG uptake values within defined subregions of the rat brain. The W. Schiffer brain VOI atlas was used in an iterative fashion with the standard brain model to further optimize the fusion of the experimental data. The regional standardized F-18 FDG uptake values ratio (SUVR) was calculated by dividing the standardized F-18 FDG uptake value for the

individual target region by that for the bilateral cerebellum.

2.6. Western blot analysis:

The expression of Bax, TNF-α, p-tau (Thr231), Aβ, Aβ40, Aβ42, and GAPDH was evaluated at 3 months after bilateral CCA ligation using western blots. The extracted brain tissue (left temporal cortex, and hippocampus) from the 15 rats in each experimental group was homogenized with T-PERTM Tissue Protein Extraction Reagent (78510; Thermo Fisher Scientific, Waltham, MA, USA) combined with proteinase inhibitor cocktail tablet 1 (cOmplete Mini, EDTA-free; Roche Applied Science, Germany) and PhosSTOP EASY (Roche Applied Science, Germany) and then incubated at 4 ℃ for 30 min. Samples were then centrifuged at 15,000 rpm for 15 min at 4 ℃. The amount of protein (10 μg) was estimated using a bicinchoninic acid assay protein assay (Pierce, Thermo Fisher Scientific, Waltham, MA, USA). Proteins separated using 10% sodium dodecyl sulfate-polyacrylamide gel electrophoresis were transferred to nitrocellulose membranes, and immunoreactive bands were visualized using a chemiluminescent reagent (SuperSignal West Femto Maximum Sensitivity Substrate; Thermo Fisher Scientific, Waltham, MA, USA). The signals of the bands were quantified with the scion image software using a FUSIONSOLO5 (KOREA BIOMICS, Korea). The following antibodies were used: anti-bax (1:1000) (ab182733, Abcam, Cambridge, MA, USA), anti-TNF-α (1:1000) (ab6671, Abcam, Cambridge, MA, USA), anti-hyperphosphorylated tau (1:1000) (ab151559, Abcam, Cambridge, MA, USA), anti- Amyloid β (ab216436, Abcam, Cambridge, MA, USA), anti-Amyloid β1-40 (1:1000) (ab17295, Abcam, Cambridge, MA, USA),

anti-Amyloid β1-42 (1:1000) (ab201061, Abcam, Cambridge, MA, USA), anti-GAPDH (1:2000) (2118, Cell Signaling Technology, Danvers, MA, USA), anti-mouse IgG HRP-linked antibody (1:1000) (Santa Cruz Biotechnology, Santa Cruz, CA, USA), and anti-rabbit IgG HRP-linked antibody (1:1000) (Santa Cruz Biotechnology, Santa Cruz, CA, USA).

2.7. Y-maze test:

The Y-maze test was performed to assess recognition memory from the 15 rats in each experimental group as described previously (25). The apparatus for the Y-maze comprised three arms (500 mm long, 150 mm high, and 100 mm wide; labeled A, B, and C) diverging at a 120 ° angle. The Y-maze test was performed in a dimly illuminated testing room 3 months after surgery. Rats moved into the room and allowed them to adapt for 1 h. Each rat was gently placed at the end of start arm and allowed to freely move through the Y-maze for 10 min without reinforcers, such as food, water, or electric shock. During the test, the operator was blinded to the group allocation of each animal and the behaviors of the rats were recorded using a video camera. The floor of the maze was cleaned with 70% ethanol after each rat was tested to avoid olfactory cues. An actual alternation was defined as consecutive entries into all three arms. The maximum number of alternations was then calculated by subtracting two units from the total number of arm entries, and the percentage of spontaneous alternation was calculated as follows: spontaneous alternation (%) = (actual number of alternations/maximum number of alternations) × 100 (26). The total number of arms entered during the test was also recorded.

2.8 Statistical analysis:

The results are expressed as the mean ± standard deviation (SD). Statistical Package for the Social Sciences (SPSS) software version 26.0 (IBM corporation, Armonk, NY, USA) was used for the statistical analyses. Differences in CBF; infarct volume; regional SUVR; Bax, TNF-α, p-tau (Thr231), Aβ, Aβ40 and Aβ42 expression levels; and the recognition index between the CAL and control groups were evaluated using the Student's two-tailed *t*-test. A value of $p < 0.05$ was considered statistically significant.

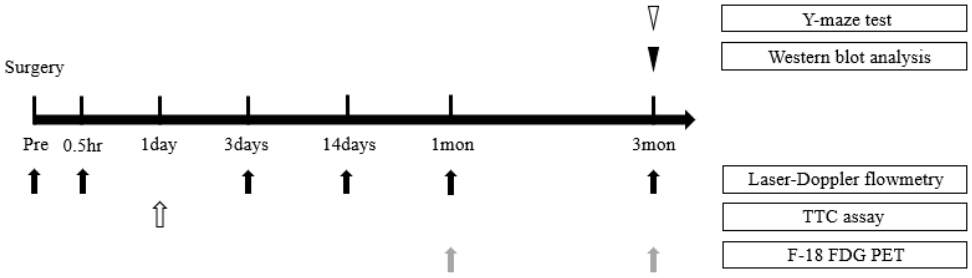

Figure 1. Experimental design. CAL and control groups were performed in 11-week-old Wistar rats. To confirm that there was no cerebral infarction after surgery, TTC assay performed on 7 rats in each group randomly, immediately after surgery. F-18 FDG PET imaging was performed 1 and 3 months after surgery. The Y-maze test and western blot analysis were performed 3 months after surgery. CAL: bilateral common carotid artery ligation; TTC: 2,3,5-triphenyltetrazolium chloride; F-18 FDG: F-18 fluorodeoxyglucose; PET: positron emission tomography.

3. Results

3.1. Chronic cerebral hypoperfusion:

Using laser-Doppler flowmetry, the CBF was measured just before and at 30 min, 3 days, 14 days, 1 month, and 3 months after the bilateral CCA ligation (Figure 2). At 30 min and 3 days after the surgery, there was a significant decrease in the CBF ratio in the CAL group compared with that in the control group (43.2 ± 7.3% vs. 97.1 ± 9.6%, $p < 0.001$ and 32.4 ± 9.2% vs. 98.1 ± 5.1%, $p < 0.001$, respectively). At 14 days, the CBF ratio of the CAL group began to recover but remained significantly lower than that of the control group (71.3 ± 14.3% vs. 98.9 ± 2.9%, $p < 0.001$). At 3 months, the CBF ratio of the CAL group was slightly increased compared to that of the control group (106.2 ± 5.8% vs. 99.0 ± 3.4%, $p < 0.001$).

The TTC assay showed that there was no cerebral infarct in the bilateral cerebral hemisphere in both the control and CAL groups (Figure 3).

3.2. Cerebral glucose metabolism:

At 1 month after the ligation, the SUVRs of the left entorhinal cortex, bilateral frontal association cortex, right motor cortex, and left somatosensory cortex were significantly lower in the CAL group than those in the control group ($p < 0.05$, $p < 0.05$, $p < 0.01$, $p < 0.05$, and $p < 0.05$, respectively; Figure 4). However, there were no significant differences in the SUVR in other regions of the brain at 1 month

(Table 1). At 3 months after the ligation, only the SUVR of the right anterodorsal hippocampus was significantly lower in the CAL group compared with that of the control group ($p < 0.05$; Figure 4). There were no significant differences in any other regions between the control and the CAL groups at 3 months after the ligation (Table 1).

3.3. Development of AD pathology:

Western blot analysis was conducted 3 months after the ligation to determine the protein expression levels of Bax, TNF-α, p-tau, Aβ, Aβ 40, Aβ42, and GAPDH in the hippocampus and temporal cortex. In the hippocampus, the expression of Aβ42 was significantly increased in the CAL group compared with that in the control group ($p < 0.05$) (Figure 5). Moreover, the Aβ42/40 ratio in the hippocampus of the CAL group was significantly elevated in comparison to that of the control group ($p < 0.05$). The p-tau levels of the hippocampus in the CAL group were significantly lower as compared with those of the control group ($p < 0.05$). There were no significant differences in the expression levels of Bax, TNF-α, Aβ, and Aβ40 in the hippocampus between the two groups. In the temporal cortex, the expression levels of Bax, TNF-α, p-tau, Aβ, Aβ40, and Aβ42, and the Aβ42/40 ratio were not significantly different between the CAL and the control groups (Figure 6).

3.4. Recognition memory:

The Y-maze test was performed 3 months after surgery to assess recognition memory. There was no difference in the number of arm

entries between the control and the CAL groups. In contrast, there was significantly lower spontaneous alternation in the CAL group compared with the control group at 3 months (71.42 ± 9.89% vs. 59.39 ± 8.59%, $p < 0.05$; Figure 7).

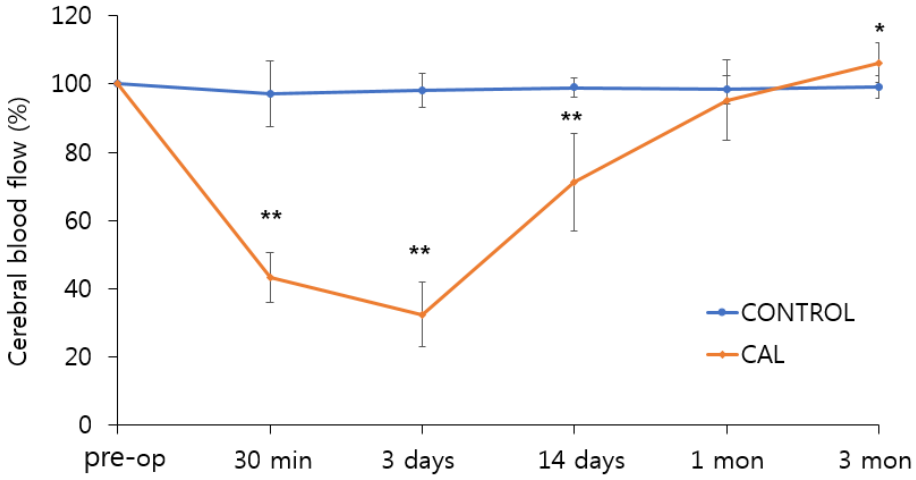

Figure 2. Comparison of cerebral blood flow (CBF) between the bilateral common carotid artery ligation (CAL) and control groups. The CBF was measured before and at 30 min, 3 days, 14 days, 1 month, and 3 months after CAL surgery, and in the control group using laser-Doppler flowmetry. At both 30 min and 3 days after surgery, there was a significant decrease in the CBF ratio in the CAL group compared with that in the control group. At 14 days, the CBF ratio in the CAL group began to recover but remained significantly lower than that in the control group. In contrast, the CBF ratio in the CAL group was slightly but significantly increased compared with that of the control group at 3 months after surgery. Asterisks indicate statistical significance: $^{**}p < 0.01$ $^{*}p < 0.05$.

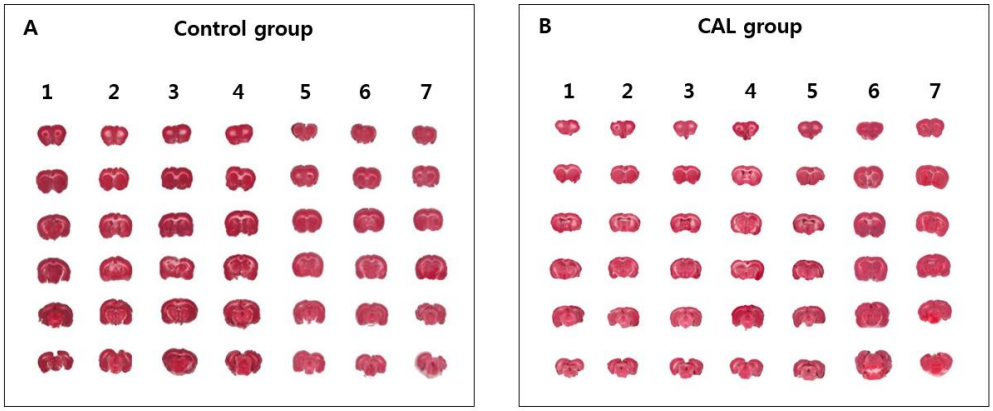

Figure 3. Comparison of cerebral infarct volume between the bilateral common carotid artery ligation (CAL) and control groups. Cerebral infarct volume was evaluated by the 2,3,5-triphenyltetrazolium chloride (TTC) assay. (A) TTC assay showing that none of the seven rats in the control group exhibited cerebral infarction. (B) In the CAL group, none of the seven rats exhibited a cerebral infarct.

Table 1. Comparison of Regional Cerebral Glucose Metabolism at 1 and 3 Months after Surgery

Regions	Side	1 Month		p value	3 Months		p value
		Control	CAL		Control	CAL	
Accumbens	left	1.02 (0.09)	0.99 (0.08)	0.589	1.04 (0.10)	0.99 (0.08)	0.150
	right	1.03 (0.08)	0.98 (0.09)	0.206	1.03 (0.08)	1.02 (0.10)	0.776
Amygdala	left	0.89 (0.05)	0.84 (0.06)	0.070	0.87 (0.07)	0.83 (0.07)	0.122
	right	0.88 (0.06)	0.87 (0.08)	0.945	0.86 (0.05)	0.83 (0.05)	0.162
Auditory cortex	left	0.89 (0.09)	0.82 (0.08)	0.084	0.92 (0.07)	0.89 (0.08)	0.189
	right	0.86 (0.08)	0.79 (0.11)	0.111	0.89 (0.06)	0.86 (0.07)	0.198
Cingulate cortex	left	1.07 (0.15)	0.95 (0.09)	0.050	1.06 (0.11)	1.00 (0.12)	0.116
	right	1.05 (0.15)	0.94 (0.10)	0.081	1.05 (0.10)	1.01 (0.15)	0.300
Entorhinal cortex	left	0.89 (0.06)	0.83 (0.07)	0.036*	0.88 (0.06)	0.87 (0.08)	0.732
	right	0.89 (0.08)	0.83 (0.07)	0.081	0.88 (0.07)	0.88 (0.08)	0.918
Frontal association cortex	left	0.95 (0.09)	0.84 (0.09)	0.023*	0.89 (0.10)	0.87 (0.09)	0.708
	right	0.91 (0.08)	0.78 (0.09)	0.005*	0.88 (0.10)	0.86 (0.08)	0.563
Insular cortex	left	0.97 (0.10)	0.89 (0.08)	0.059	0.98 (0.07)	0.96 (0.06)	0.493
	right	0.95 (0.09)	0.89 (0.08)	0.119	0.96 (0.07)	0.97 (0.10)	0.729
Medial prefrontal cortex	left	1.14 (0.16)	1.04 (0.09)	0.102	1.17 (0.13)	1.11 (0.17)	0.259
	right	1.10 (0.14)	1.02 (0.10)	0.181	1.16 (0.13)	1.13 (0.20)	0.627
Motor cortex	left	0.94 (0.10)	0.86 (0.07)	0.088	0.94 (0.09)	0.93 (0.08)	0.575
	right	0.94 (0.08)	0.85 (0.10)	0.047	0.92 (0.06)	0.91 (0.09)	0.718
Orbitofrontal cortex	left	1.04 (0.10)	0.96 (0.09)	0.083	1.03 (0.09)	1.00 (0.09)	0.321
	right	1.01 (0.10)	0.94 (0.08)	0.099	1.02 (0.08)	0.98 (0.09)	0.128
Paracortex	left	0.85 (0.08)	0.80 (0.04)	0.108	0.87 (0.09)	0.88 (0.09)	0.776
	right	0.85 (0.08)	0.78 (0.12)	0.151	0.85 (0.08)	0.82 (0.08)	0.287
Retrosplenial cortex	left	0.93 (0.09)	0.89 (0.08)	0.327	0.95 (0.07)	0.93 (0.12)	0.484
	right	0.93 (0.08)	0.87 (0.06)	0.118	0.96 (0.08)	0.90 (0.09)	0.077
Somatosensory cortex	left	0.92 (0.08)	0.85 (0.06)	0.043*	0.92 (0.06)	0.93 (0.07)	0.638
	right	0.91 (0.06)	0.84 (0.11)	0.095	0.89 (0.06)	0.90 (0.07)	0.888
Visual cortex	left	0.87 (0.08)	0.81 (0.06)	0.152	0.89 (0.09)	0.89 (0.09)	0.920
	right	0.86 (0.08)	0.79 (0.10)	0.139	0.86 (0.08)	0.84 (0.08)	0.370
Anterodorsal hippocampus	left	1.03 (0.07)	0.98 (0.07)	0.160	1.03 (0.07)	1.02 (0.08)	0.586
	right	1.03 (0.07)	0.99 (0.09)	0.233	1.03 (0.07)	0.96 (0.09)	0.014*
Posterior hippocampus	left	0.96 (0.06)	0.96 (0.05)	0.831	0.94 (0.05)	0.92 (0.07)	0.491
	right	0.94 (0.06)	0.96 (0.11)	0.632	0.95 (0.05)	0.95 (0.09)	0.864

Asterisks indicate statistical significance: $^{*}p < 0.05$ CAL: bilateral common carotid artery ligation.

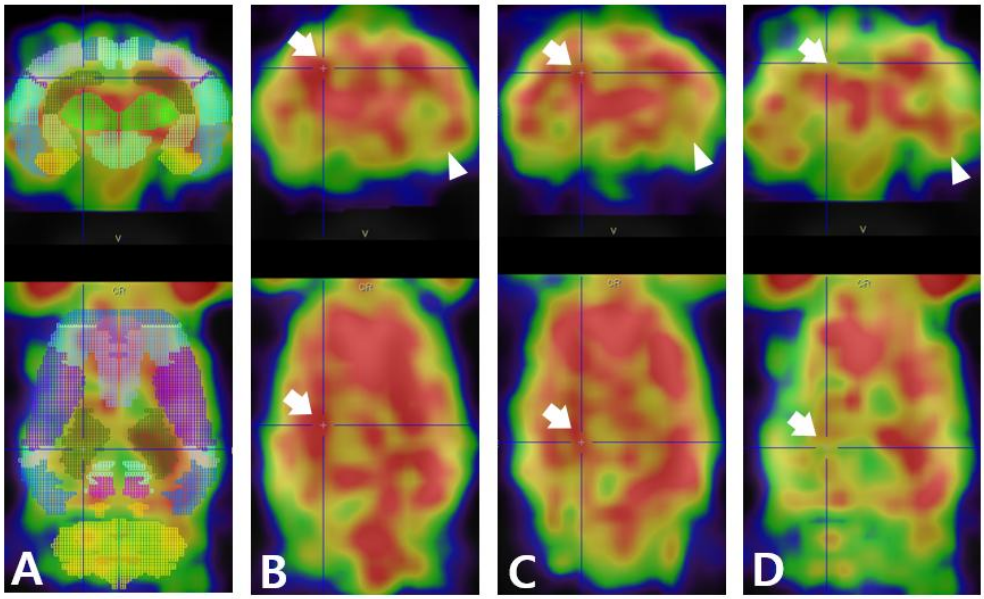

Figure 4. Cerebral glucose metabolism measured by F-18 FDG PET. (A) Regional SUVRs were obtained from the W. Schiffer rat brain VOI analysis using the PMOD software package (see Methods). (B) No abnormal glucose metabolism of the right anterodorsal hippocampus (arrow) and left entorhinal cortex (arrow head) is visible in a control group. (C) Decreased glucose metabolism of the left entorhinal cortex but not the right anterodorsal hippocampus is visible in a rat with bilateral CCA ligation after 1 month (CAL group). (D) 3 months after bilateral common CCA (CAL group), decreased glucose metabolism is only visible in the right anterodorsal hippocampus. F-18 FDG: F-18 fluorodeoxyglucose; PET: positron emission tomography. SUVR: standardized F-18 FDG uptake values ratio; VOI: volume-of interest; CCA: common carotid artery; CAL: bilateral common carotid artery ligation.

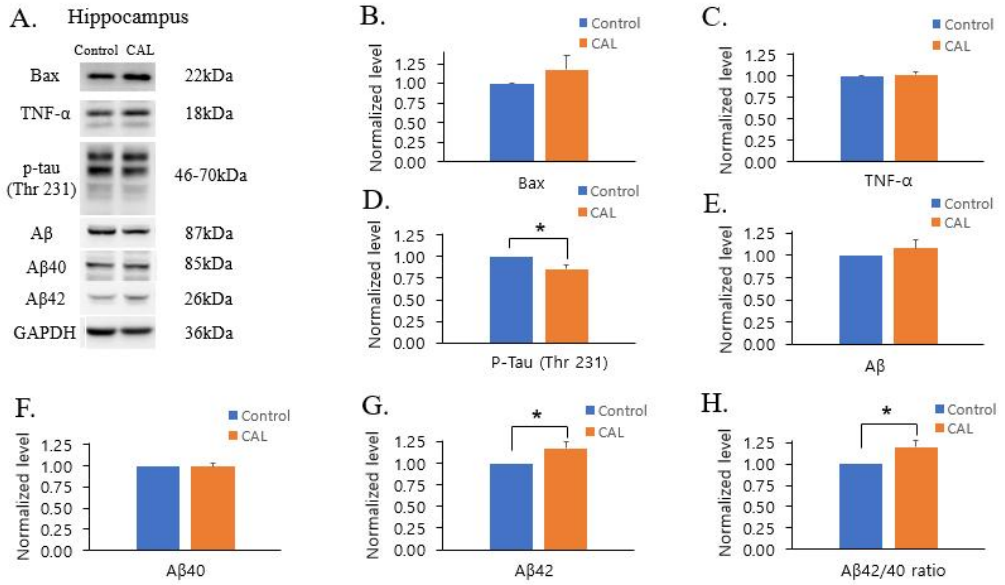

Figure 5. Comparison of Alzheimer's disease pathology in the hippocampus between the bilateral common carotid artery ligation (CAL) and control groups. (A) The expression levels of Bax, TNF-α, hyperphosphorylated tau (p-tau), amyloid β (Aβ), amyloid β40 (Aβ40), and amyloid β42 (Aβ 42) were evaluated in the hippocampus at 3 months after bilateral CAL using western blot analysis. (B-H) The relative ratio of Bax, TNF-α, p-tau, Aβ, Aβ40, and Aβ42 were plotted based on the quantification of band intensity using scion image software. Values are expressed as the mean ± SD. Asterisks indicate statistical significance: $^{*}p < 0.05$.

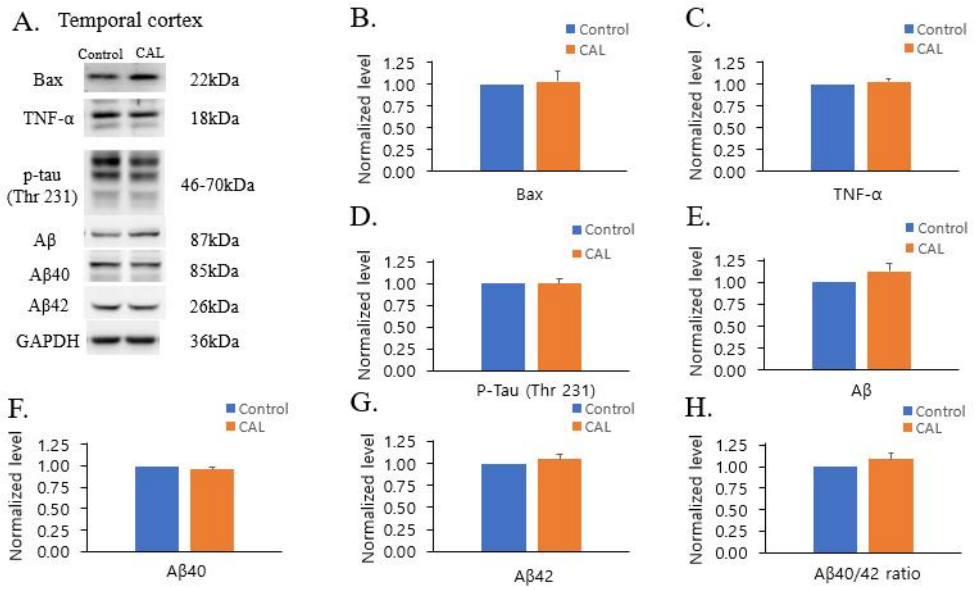

Figure 6. Comparison of AD pathology between the bilateral common carotid artery ligation (CAL) and control groups in the temporal cortex. (A) The expression levels of Bax, TNF-α, hyperphosphorylated tau (p-tau), amyloid β (Aβ), amyloid β 40 (Aβ40), and amyloid β42 (Aβ42) were evaluated in the temporal cortex at 3 months after bilateral CAL using western blot analysis. (B-H) The relative ratio of Bax, TNF-α, p-tau, Aβ, Aβ40, and Aβ42 were plotted based on the quantification of band intensity using scion image software. Values are expressed as the mean ± SD.

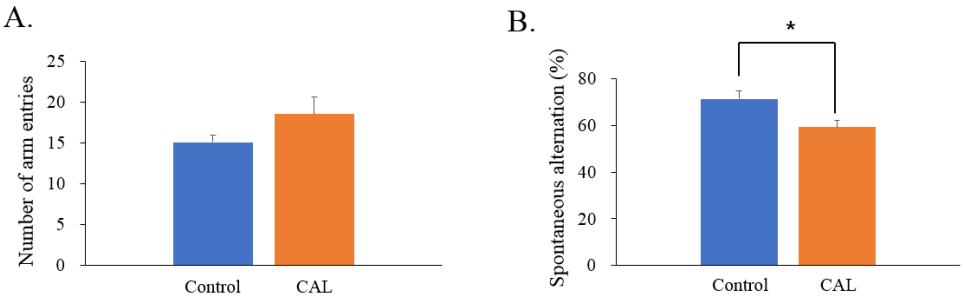

Figure 7. Comparison of recognition memory assessed by the Y-maze test between the bilateral common carotid artery ligation (CAL) and control groups. The number of arm entries (A) and alternation behaviors (B) measured after 3 months in the bilateral common carotid artery ligation (CAL group) and control group are shown. Asterisks indicate statistical significance: $^{*}p < 0.05$.

4. Discussion

The present study showed that CCH decrease the neuronal activity of the hippocampus, causing cognitive decline in a rat model. The results also showed that CCH induces cerebral Aβ accumulation. These results suggest that CCH causes selective hippocampal degeneration, which induces AD pathology. The present study helps to understand the mechanism by which cerebrovascular disease contributes to AD development.

CCH by permanent bilateral CCA ligation offers several advantages compared to other approaches. It can induce CCH in a more clinically relevant manner, without ischemic lesions in the brain (27, 28). The present study induced CCH by CCA ligation in the rat brain using real time CBF monitoring, and there was no ischemic lesion in the brain. The CBF monitoring revealed a sharp decrease in the early stages after surgery, resulting in a 68% and 29% decrease in CBF at 3 and 14 days after the surgery, respectively. The CBF gradually recovered from the 14th day after surgery and reached a normal level at 1 month. In agreement with our results, a previous study with rats reported that bilateral occlusion of the CCA led to a dramatic initial drop in CBF, which subsequently returned to 30-45% CBF in the cortex and a 20% reduction in the hippocampus 1 week after surgery (29). The gradual recovery of the CBF could be caused by supply from the collateral blood vessels, such as through the posterior communicating artery (23).

Several studies of patients with late stage of AD have reported decreased cerebral glucose metabolism in the temporal and parietal cortices, posterior cingulate, and precuneus (30). Moreover, in the early stage of AD, decreased cerebral glucose metabolism has been observed

in the hippocampus, and hippocampal dysfunction has been shown to be associated with that of the parietal and temporal cortices, suggesting that hippocampal degeneration could be an important trigger for the onset of AD (31). A recent study using high-resolution F-18 FDG PET and magnetic resonance imaging (MRI) reported decreased glucose metabolism in the bilateral hippocampus in patients with early-stage AD (32). An MRI study has identified hippocampal atrophy as an early sign of AD (33). Further, another MRI study revealed that hippocampal atrophy is independently associated with the progression to AD (34). In accordance with these previous studies, the present study revealed that glucose metabolism in the anterodorsal hippocampus was decreased by CCH 3 months after the surgery; however, glucose metabolism in all other regions had recovered. It is known that the hippocampus, which is involved in memory formation, is susceptible to ischemia (35). The selective decrease in glucose metabolism in the hippocampus could be due to this vulnerability to ischemic insults (36). Previous studies using animal models have reported that the hippocampus is particularly vulnerable to ischemia, supporting the ischemic hypothesis for AD development in terms of CCH (37).

A previous study of ischemic animal models has revealed that CCH can induce AD pathology (38). A study using specific enzyme-linked immunosorbent assays reported that white matter hyperintensities were significantly associated with plasma Aβ40 and Aβ42 levels in an AD and mild cognitive impairment population (39). In agreement with previous studies, the present study showed that the expression levels of Aβ42 and the Aβ42/40 ratio were increased in the hippocampus 3 months after bilateral CCA ligation. Thus, chronic ischemia mechanically contributes to the development of AD through alteration of Aβ metabolism was postulated. In mutant APP transgenic mice, long-term

hypoxia has been shown to contribute to increased Aβ deposition and neuritic plaque formation, potentiating memory deficit by increasing the transcription and expression of the β-site APP cleaving enzyme 1 (BACE1) gene, which is primarily mediated by the binding of hypoxia-inducible factor-1α to the BACE1 promoter (40, 41). Further, BACE1 activation and resultant Aβ40 overproduction have been reported in Tg2576 mice following energy insufficiency induced by pharmacological agents (e.g. insulin, 2-deoxyglucose, 3-nitropropionic acid, or kainic acid) (42). These findings collectively suggest that energy/oxygen deficiency facilitates AD pathogenesis via increased BACE1 expression and Aβ overproduction.

The present study utilized the Y-maze test to evaluate the learning and memory skills in the control and CAL rats. The Y-maze test can specifically evaluate hippocampus-dependent short-term and spatial memory processing, which is particularly affected by AD (43). The present study revealed that CCH and decreased metabolism in the hippocampus aggravates memory impairment on the Y-maze test. A Rotterdam Study of 1,730 participants suggested that CCH precedes and possibly contributes to the onset of clinical dementia (44). In an animal study of APPswe/PS1 mice, CCH induced by single vessel occlusion has been shown to exacerbate memory deficits (45, 46). Another study using the J20/APP AD mouse model showed that CCH induced by bilateral carotid artery stenosis exacerbated learning impairment (15). The memory impairment induced by CCH is presumed to be caused by hippocampal degeneration. The hippocampus is one of the cerebral structures that undergoes neurodegenerative changes in the early stages of AD (47, 48). Hippocampal formation is involved in the learning process and plays an important role in processing and remembering spatial and contextual information (49). In patients with AD, progressive

hippocampal dysfunction has been reported to cause memory impairment (50), which was consistent with our results.

The current study has some limitations. First, the mechanism by which selective hippocampal degeneration causes AD pathology has not been identified. Further, it is unclear whether CCH generates AD pathology directly or in combination with other causes. Second, our animal model did not have persistent CCH, because the CBF recovered to normal values 1 month after the bilateral CAL surgery. Persistent CCH would likely reveal the effect on AD development more clearly, and would be more consistent with the clinical situation. Animal models of diabetes with a high-fat diet or type-I interferon injection have been shown cause small vessel disease or multivessel atherosclerosis resulting in CCH (51). Thus, further studies using these animal models are needed to demonstrate the effect of CCH on AD development. Finally, the mechanism by which CCH affects AD development, along with other complex causes, and how to prevent AD development or slow AD progression by inhibiting this process should be studied in the future.

In conclusion, CCH induces the AD pathology with selectively degeneration of the hippocampus in rats. CCH may play a significant role in the development of AD and the selective neurodegeneration of the hippocampus may be a trigger point for the development of AD pathology. Further studies are needed to elucidate the mechanisms by which CCH aggravates AD pathology.

5. Summary

This present study demonstrated that CCH induces AD pathology with selective degeneration of the hippocampus in rats. At 1 month after the bilateral CCA ligation in rats, cerebral glucose metabolism in the entorhinal, frontal association, motor, and somatosensory cortices were significantly decreased in the CAL group compared with those in the control group. At 3 months after the ligation, cerebral glucose metabolism in CAL group was normalized in all regions except for the anterodorsal hippocampus, which was significantly decreased compared with that of the control group. In addition, Aβ42 levels and Aβ42/40 ratios were increased in the hippocampus of the CAL group. CCH would play an important role in the development of AD. The selective neurodegeneration of the hippocampus may be a trigger point for the development of AD pathology.

References

1. Ferri CP, Prince M, Brayne C, Brodaty H, Fratiglioni L, Ganguli M, et al.: Global prevalence of dementia: a Delphi consensus study. Lancet 2005; 366: 2112-7.

2. Nelson PT, Alafuzoff I, Bigio EH, Bouras C, Braak H, Cairns NJ, et al.: Correlation of Alzheimer disease neuropathologic changes with cognitive status: a review of the literature. J Neuropathol Exp Neurol 2012; 71: 362-81.

3. Murphy MP, LeVine H 3rd: Alzheimer's disease and the amyloid-beta peptide. J Alzheimers Dis 2010; 19: 311-23.

4. Koike MA, Green KN, Blurton-Jones M, Laferla FM: Oligemic hypoperfusion differentially affects tau and amyloid-beta. Am J Pathol 2010; 177: 300-10.

5. de la Torre JC: Alzheimer disease as a vascular disorder: nosological evidence. Stroke 2002; 33: 1152-62.

6. Kalaria RN: Cerebral vessels in ageing and Alzheimer's disease. Pharmacol Ther 1996; 72: 193-214.

7. Thal DR, Griffin WST, de Vos RAI, Ghebremedhin E: Cerebral amyloid angiopathy and its relationship to Alzheimer's disease. Acta Neuropathol 2008; 115: 599-609.

8. Massaad CA: Neuronal and vascular oxidative stress in Alzheimer's disease. Curr neuropharmacol 2011; 9: 662-73.

9. Popa-Wagner A, Mitran S, Sivanesan S, Chang E, Buga AM: ROS and brain diseases: the good, the bad, and the ugly. Oxid Med Cell Longev 2013; 2013: 963520.

10. Safouris A, Hambye AS, Sculier C, Papageorgiou SG, Vasdekis SN, Gazagnes MD, et al.: Chronic brain hypoperfusion due to multi-vessel extracranial atherosclerotic disease: a potentially reversible cause of cognitive impairment. J Alzheimers Dis 2015; 43: 23-7.

11. Deb P, Sharma S, Hassan KM: Pathophysiologic mechanisms of acute ischemic stroke: An overview with emphasis on therapeutic significance beyond thrombolysis. Pathophysiology 2010; 17: 197-218.

12. Broughton BR, Reutens DC, Sobey CG: Apoptotic mechanisms after cerebral ischemia. Stroke 2009; 40: e331-9.

13. Iadecola C: The pathobiology of vascular dementia. Neuron 2013; 80: 844-66.

14. Okamoto Y, Yamamoto T, Kalaria RN, Senzaki H, Maki T, Hase Y, et al.: Cerebral hypoperfusion accelerates cerebral amyloid angiopathy and promotes cortical microinfarcts. Acta neuropathol 2012; 123: 381-94.

15. Yamada M, Ihara M, Okamoto Y, Maki T, Washida K, Kitamura A, et al.: The influence of chronic cerebral hypoperfusion on cognitive function and amyloid β metabolism in APP overexpressing mice. PLoS one 2011; 6: e16567.

16. Yata K, Tomimoto H: Chronic cerebral hypoperfusion and dementia. Neurol Clin Neurosci 2014; 2: 129-34.

17. Sokoloff L, Reivich M, Kennedy C, Rosiers MHD, Patlak CS, Pettigrew KD, et al.: The [^{14}C]deoxyglucose method for measurement of local cerebral glucose utilization: theory, procedure, and normal values in the conscious and anesthetized albino rat. J Neurochem 1977; 28: 897-916.

18. Haass C, Selkoe DJ: Soluble protein oligomers in neurodegeneration: lessons from the Alzheimer's amyloid beta-peptide. Nat Rev Mol Cell Biol 2007; 8: 101-12.

19. Drzezga A, Becker JA, Van Dijk KRA, Sreenivasan A, Talukdar T, Sullivan C, et al.: Neuronal dysfunction and disconnection of cortical hubs in non-demented subjects with elevated amyloid burden. Brain 2011; 134: 1635-46.

20. Meguro K, Blaizot X, Kondoh Y, Le Mestric C, Baron JC, Chavoix C: Neocortical and hippocampal glucose hypometabolism following neurotoxic lesions of the entorhinal and perirhinal cortices in the non-human primate as shown by PET: Implications for Alzheimer's disease. Brain 1999; 122: 1519-31.

21. Lu Y, Ren J, Cui S, Chen J, Huang Y, Tang C, et al.: Cerebral glucose metabolism assessment in rat models of Alzheimer's disease: An ^{18}F-FDG-PET study. Am J Alzheimers Dis Other Demen 2016; 31: 333-40.

22. Park JH, Hong JH, Lee SW, Ji HD, Jung JA, Yoon KW, et al.: The effect of chronic cerebral hypoperfusion on the pathology of Alzheimer's disease: A positron emission tomography study in rats. Sci Rep 2019; 9: 14102.

23. Shibata M, Ohtani R, Ihara M, Tomimoto H: White matter lesions and glial activation in a novel mouse model of chronic cerebral hypoperfusion. Stroke 2004; 35: 2598-603.

24. Balsara RD, Chapman SE, Sander IM, Donahue DL, Liepert L, Castellino FJ, et al.: Non-invasive imaging and analysis of cerebral ischemia in living rats using positron emission tomography with ^{18}F-FDG. J Vis Exp 2014; 94: 51495.

25. Mulas A, Crabai F, Pepeu G: The influence of repeated experience on the effects of scopolamine and of amphetamine on exploratory behaviour in the rat. Pharmacol Res Commun 1970; 2: 169-76.

26. Miedel CJ, Patton JM, Miedel AN, Miedel ES, Levenson JM: Assessment of spontaneous alternation, novel object recognition and limb clasping in transgenic mouse models of amyloid-β and tau neuropathology. J Vis Exp 2017; 123: e55523.

27. Yang G, Kitagawa K, Matsushita K, Mabuchi T, Yagita Y,

Yanagihara T, et al.: C57BL/6 strain is most susceptible to cerebral ischemia following bilateral common carotid occlusion among seven mouse strains: selective neuronal death in the murine transient forebrain ischemia. Brain Res 1997; 752: 209-18.

28. Toyama K, Koibuchi N, Uekawa K, Hasegawa Y, Kataoka K, Katayama T, et al.: Apoptosis signal-regulating kinase 1 is a novel target molecule for cognitive impairment induced by chronic cerebral hypoperfusion. Arterioscler Thromb Vasc Biol 2014; 34: 616-25.

29. Tsuchiya M, Sako K, Yura S, Yonemasu Y: Cerebral blood flow and histopathological changes following permanent bilateral carotid artery ligation in wistar rats. Exp Brain Res 1992; 89: 87-92.

30. Nasrallah IM, Wolk DA: Multimodality imaging of Alzheimer disease and other neurodegenerative dementias. J Nucl Med 2014; 55: 2003-11.

31. Bruner E, Jacobs HIL: Alzheimer's disease: the downside of a highly evolved parietal lobe? J Alzheimers Dis 2013; 35: 227-40.

32. Choi EJ, Son YD, Noh Y, Lee H, Kim YB, Park KH: Glucose hypometabolism in hippocampal subdivisions in Alzheimer's disease: A pilot study using high-resolution ^{18}F-FDG PET and 7.0-T MRI. J Clin Neurol 2018; 14: 158-64.

33. Frisoni GB, Fox NC, Jack CR Jr, Scheltens P, Thompson PM: The clinical use of structural MRI in Alzheimer disease. Nat Rev Neurol 2010; 6: 67-77.

34. Brickman AM, Zahodne LB, Guzman VA, Narkhede A, Meier IB, Griffith EY, et al.: Reconsidering harbingers of dementia: progression of parietal lobe white matter hyperintensities predicts Alzheimer's disease incidence. Neurobiol Aging 2015; 36: 27-32.

35. Bekinschtein P, Katche C, Slipczuk LN, Igaz LM, Cammarota M, Izquierdo I, et al.: mTOR signaling in the hippocampus is necessary for memory formation. Neurobiol Learn Mem 2007; 87: 303-7.

36. Zhu H, Yoshimoto T, Imajo-Ohmi S, Dazortsava M, Mathivanan A, Yamashima T: Why are hippocampal CA1 neurons vulnerable but motor cortex neurons resistant to transient ischemia? J Neurochem 2012; 120: 574-85.

37. Schmidt-Kastner R: Genomic approach to selective vulnerability of the hippocampus in brain ischemia - hypoxia. Neuroscience 2015; 309: 259-79.

38. Zhao Y, Gong C-X: From chronic cerebral hypoperfusion to Alzheimer-like brain pathology and neurodegeneration. Cell Mol Neurobiol 2015; 35: 101-10.

39. Gurol ME, Irizarry MC, Smith EE, Raju S, Diaz-Arrastia R, Bottiglieri T, et al.: Plasma β-amyloid and white matter lesions in AD, MCI, and cerebral amyloid angiopathy. Neurology 2006; 66: 23-9.

40. Sun X, He G, Qing H, Zhou W, Dobie F, Cai F, et al.: Hypoxia

facilitates Alzheimer's disease pathogenesis by up-regulating BACE1 gene expression. Proc Natl Acad Sci U S A 2006; 103: 18727-32.

41. Zhang X, Zhou K, Wang R, Cui J, Lipton SA, Liao F-F, et al.: Hypoxia-inducible factor 1α (HIF-1α)-mediated hypoxia increases BACE1 expression and β-Amyloid generation. J Biol Chem 2007; 282: 10873-80.

42. Velliquette RA, O'Connor T, Vassar R: Energy inhibition elevates beta-secretase levels and activity and is potentially amyloidogenic in APP transgenic mice: possible early events in Alzheimer's disease pathogenesis. J Neurosci 2005; 25: 10874-83.

43. Kraeuter A-K, Guest PC, Sarnyai Z: The Y-maze for assessment of spatial working and reference memory in mice. Methods Mol Biol 2019; 1916: 105-11.

44. Ruitenberg A, den Heijer T, Bakker SL, van Swieten JC, Koudstaal PJ, Hofman A, et al.: Cerebral hypoperfusion and clinical onset of dementia: the Rotterdam study. Ann Neurol 2005; 57: 789-94.

45. Lee JS, Im DS, An YS, Hong JM, Gwag BJ, Joo IS: Chronic cerebral hypoperfusion in a mouse model of Alzheimer's disease: an additional contributing factor of cognitive impairment. Neurosci Lett 2011; 489: 84-8.

46. Pimentel-Coelho PM, Michaud J-P, Rivest S: Effects of mild chronic cerebral hypoperfusion and early amyloid pathology on spatial learning and the cellular innate immune response in mice. Neurobiol

Aging 2013; 34: 679-93.

47. Braak H, Braak E: Neuropathological stageing of Alzheimer-related changes. Acta Neuropathol 1991; 82: 239-59.

48. Mufson EJ, He B, Nadeem M, Perez SE, Counts SE, Leurgans S, et al.: Hippocampal proNGF signaling pathways and β-amyloid levels in mild cognitive impairment and Alzheimer disease. J Neuropathol Exp Neurol 2012; 71: 1018-29.

49. Jarrard LE: On the role of the hippocampus in learning and memory in the rat. Behav Neural Biol 1993; 60: 9-26.

50. Escribano L, Simón A-M, Pérez-Mediavilla A, Salazar-Colocho P, Río JD, Frechilla D: Rosiglitazone reverses memory decline and hippocampal glucocorticoid receptor down-regulation in an Alzheimer's disease mouse model. Biochem Biophys Res Commun 2009; 379: 406-10.

51. Kivipelto M, Helkala EL, Laakso MP, Hänninen T, Hallikainen M, Alhainen K, et al.: Midlife vascular risk factors and Alzheimer's disease in later life: longitudinal, population based study. Br Med J 2001; 322: 1447-51.

Selective Neurodegeneration of the Hippocampus Caused by Chronic Cerebral Hypoperfusion : F-18 FDG PET Study in Rats

Lee, Jung In

Department of Nuclear Medicine
Graduate School

Keimyung University

(Supervised by Professor Kim, Hae Won)

(Abstract)

Cerebrovascular disease is a potential risk factor for Alzheimer's disease (AD). Chronic cerebral hypoperfusion (CCH) is known to induce AD pathology, but its mechanism remains unclear. The purpose of this study was to identify the cerebral regions affected by CCH causing AD pathology. A rat model of CCH was established by bilaterally ligating the common carotid arteries (CCA) in adult male rats (CAL group). Sham-operated rats underwent the same procedures without artery ligation (control group). Regional cerebral glucose metabolism was evaluated at 1 and 3 months after bilateral CCA ligation using positron emission tomography with F-18 fluorodeoxyglucose. The expression levels of amyloid β40 (Aβ40), amyloid β42 (Aβ42), and

hyperphosphorylated tau were evaluated using western blots at 3 months after the ligation. Cognitive function was evaluated using the Y-maze test at 3 months after the ligation. At 1 month after the ligation, cerebral glucose metabolism in the entorhinal, frontal association, motor, and somatosensory cortices were significantly decreased in the CAL group compared with those in the control group. At 3 months after the ligation, cerebral glucose metabolism was normalized in all regions except for the anterodorsal hippocampus, which was significantly decreased compared with that of the control group. The expression of Aβ42 and the Aβ42/40 ratio were significantly higher in the CAL group than those in the control group. Cognitive function was more impaired in the CAL group than that in the control group. In conclusion, CCH causes selective neurodegeneration of the anterodorsal hippocampus, which may be a trigger point for the development of AD pathology.

만성 허혈로 인한 해마의 선택적 신경 퇴화
: F-18 FDG PET 동물 연구

이 정 인
계명대학교 대학원
의학과 핵의학 전공
(지도교수 김 해 원)

(초록)

뇌혈관 질환은 알츠하이머병의 잠재적 위험 요소이다. 만성 뇌허혈은 알츠하이머병 병리를 유발하는 것으로 알려져 있지만, 그 기전은 명확하지 않다. 이 연구의 목적은 쥐에서 알츠하이머병 병리를 일으키는 만성 뇌허혈의 영향을 받는 대뇌 영역을 탐색하는 것이었다. 만성 뇌허혈 모델은 성인 수컷 쥐(실험군)에서 양측 총경동맥을 결찰함으로써 확립되었다. 모의 수술을 받은 쥐는 동맥 결찰없이 동일한 절차를 거쳤다(대조군). 양측 총경동맥 결찰 후 1개월 및 3개월에 F-18 fluorodeoxyglucose를 사용한 양전자 방출 단층 촬영으로 대뇌 포도당 대사를 평가했다. 아밀로이드 β40(Aβ40), 아밀로이드 β42(Aβ42) 및 과인산화 타우의 발현 수준은 결찰 후 3개월에 웨스턴 블랏을 사용하여 평가되었다. 결찰 3개월 후 Y-미로 검사를 통해 인지 기능을 평가하였다. 결찰 1개월 후, 실험군의 내후각피질, 전두연합영역, 운동피질, 체성감각피질의 대뇌 포도당 대사가 대조군에 비해 유의하게 감소

하였다. 결찰 후 3개월째에, 1개월에 감소한 대뇌 포도당 대사가 정상화되었으나, 전등쪽해마의 대뇌 포도당 대사는 대조군에 비해 유의하게 감소하였다. Aβ42 및 Aβ42/40 비율의 발현은 대조군보다 실험군에서 유의하게 높았다. 또한, 실험군은 대조군보다 인지 기능 장애가 더 많았다. 결론적으로, 만성 뇌허혈은 해마의 선택적 신경 퇴행을 유발한다. 이로 인한 해마의 선택적 신경 퇴행은 알츠하이머병 병리 발생의 유발점이 될 수 있다.